The atomic structure of low-index surfaces of the intermetallic compound InPd

G. M. Mcguirk, J. Ledieu, É. Gaudry, M.-C. De Weerd, M. Hahne, P. Gille, D. Ivarsson, M. Armbrüster, J. Ardini, G. Held, et al.

The atomic structure of low-index surfaces of the intermetallic compound InPd

G. M. McGuirk, J. Ledieu, É. Gaudry, M.-C. de Weerd, M. Hahne, P. Gille, D. C. A. Ivarsson, M. Armbrüster, J. Ardini, G. Held, F. Maccherozzi, A. Bayer, M. Lowe, K. Pussi, R. D. Diehl, and V. Fournée

Citation: The Journal of Chemical Physics **143**, 074705 (2015); doi: 10.1063/1.4928650
View online: http://dx.doi.org/10.1063/1.4928650
View Table of Contents: http://scitation.aip.org/content/aip/journal/jcp/143/7?ver=pdfcov
Published by the AIP Publishing

The atomic structure of low-index surfaces of the intermetallic compound InPd

G. M. McGuirk,[1] J. Ledieu,[1] É. Gaudry,[1] M.-C. de Weerd,[1] M. Hahne,[2] P. Gille,[2] D. C. A. Ivarsson,[3] M. Armbrüster,[3] J. Ardini,[4,5] G. Held,[4,5] F. Maccherozzi,[5] A. Bayer,[6] M. Lowe,[7] K. Pussi,[8] R. D. Diehl,[9] and V. Fournée[1,a)]

[1]*Institut Jean Lamour (UMR 7198 CNRS-Université de Lorraine), Parc de Saurupt, F-54011 Nancy Cedex, France*

[2]*Department of Earth and Environmental Sciences, Crystallography Section, Ludwig-Maximilians-Universität München, Theresienstrasse 41, D-80333 München, Germany*

[3]*Faculty of Natural Sciences, Institute of Chemistry, Materials for Innovative Energy Concepts, Technische Universität Chemnitz, D-09107 Chemnitz, Germany*

[4]*Department of Chemistry, University of Reading, Reading RG6 6AD, United Kingdom*

[5]*Diamond Light Source Ltd, Didcot OX11 0DE, United Kingdom*

[6]*Lehrstuhl für Physikalische Chemie II, Universität Erlangen-Nürnberg, Egerlandstraße 3, D-91058 Erlangen, Germany*

[7]*Surface Science Research Centre and Department of Physics, The University of Liverpool, Liverpool L69 3BX, United Kingdom*

[8]*Department of Mathematics and Physics, Lappeenranta University of Technology, P.O. Box 20, FIN-53851 Lappeenranta, Finland*

[9]*Department of Physics, Penn State University, University Park, Pennsylvania 16802, USA*

(Received 24 June 2015; accepted 4 August 2015; published online 20 August 2015)

The intermetallic compound InPd (CsCl type of crystal structure with a broad compositional range) is considered as a candidate catalyst for the steam reforming of methanol. Single crystals of this phase have been grown to study the structure of its three low-index surfaces under ultra-high vacuum conditions, using low energy electron diffraction (LEED), X-ray photoemission spectroscopy (XPS), and scanning tunneling microscopy (STM). During surface preparation, preferential sputtering leads to a depletion of In within the top few layers for all three surfaces. The near-surface regions remain slightly Pd-rich until annealing to ~580 K. A transition occurs between 580 and 660 K where In segregates towards the surface and the near-surface regions become slightly In-rich above ~660 K. This transition is accompanied by a sharpening of LEED patterns and formation of flat step-terrace morphology, as observed by STM. Several superstructures have been identified for the different surfaces associated with this process. Annealing to higher temperatures (≥750 K) leads to faceting via thermal etching as shown for the (110) surface, with a bulk In composition close to the In-rich limit of the existence domain of the cubic phase. The Pd-rich InPd(111) is found to be consistent with a Pd-terminated bulk truncation model as shown by dynamical LEED analysis while, after annealing at higher temperature, the In-rich InPd(111) is consistent with an In-terminated bulk truncation, in agreement with density functional theory (DFT) calculations of the relative surface energies. More complex surface structures are observed for the (100) surface. Additionally, individual grains of a polycrystalline sample are characterized by micro-spot XPS and LEED as well as low-energy electron microscopy. Results from both individual grains and "global" measurements are interpreted based on comparison to our single crystals findings, DFT calculations and previous literature. © *2015 AIP Publishing LLC.* [http://dx.doi.org/10.1063/1.4928650]

I. INTRODUCTION

Methanol steam reforming (MSR, $CH_3OH + H_2O \rightarrow CO_2 + 3H_2$) has attracted much attention due to its potential for H_2-production for fuel applications.[1–3] The MSR reaction relies on an intricate pathway involving many intermediates. During the process, CO_2 and CO are the predominately detected gases. The former is associated with desirable H_2 production, whereas the latter degrades performance in Pt-based polymer electrolyte membrane (PEM) fuel cells.[4–7] Copper-based catalysts supported on ZnO are the most widely used catalysts although their activity decreases with time due to thermally induced sintering under reaction condition. Pd-based MSR catalysts have been widely studied following the work of Iwasa and co-workers uncovering similar catalytic activity and selectivity of Pd/ZnO, Pd/Ga_2O_3, and Pd/In_2O_3 while being more stable than Cu/ZnO.[5,8–10] The high performance of these catalysts are attributed — at least in part — to the formation of intermetallic M-Pd (M = Zn, Ga, or In) compounds by partial reduction under H_2 of the supporting oxides. Intermetallic compounds (IMCs) have ordered crystal

a)Author to whom correspondence should be addressed. Electronic mail: vincent.fournee@univ-lorraine.fr

structures that differ from those of their elemental constituents. Well-separated and catalytically active sites with uniform surrounding have been shown to be stabilized because of covalent bonding between the constituent elements.[11–13] In addition, the electronic structure of the IMC, which has a strong influence on the adsorption properties and surface reactivity of the compound, can be very different from those of the elemental constituents.[14] Therefore, a detailed knowledge of the surface atomic and electronic structure of these IMCs is highly desirable in order to understand the origin of their catalytic properties at the atomic scale.

Surfaces of ZnPd and GaPd have been investigated by means of near-surface intermetallic phases formed by depositing Zn or Ga thin films on Pd substrates followed by annealing.[6,15–21] The stoichiometric 1:1 phases can be synthesized under appropriate conditions and some structural information can be gained if a well oriented Pd single crystal is used as substrate. However, these ultra-thin films are metastable at moderate temperatures. The MSR properties of the IMCs have also been investigated by preparing single-phase polycrystalline samples and conducting near-ambient pressure X-ray photoelectron spectroscopy (NAP-XPS) with the aim to correlate the catalytic properties with the near-surface composition and the electronic structure.[22,23] No detailed structural information of the catalytic surface can be obtained in this case, due to the polycrystalline nature of the sample. Single crystals are the ultimate model systems for surface studies when available. The growth of ZnPd single crystal is difficult due to the high vapor pressure of Zn but GaPd single crystals have been successfully grown by the Czochralski method.[24] The 3-fold surfaces (111) and $(\bar{1}\bar{1}\bar{1})$ of the GaPd IMC have been investigated recently showing that these model surfaces exhibit small and well-defined ensembles of active metal atoms, thus fulfilling the site isolation concept.[25–27]

The InPd system has been investigated more recently. NAP-XPS was used to study the composition, the electronic structure, and the catalytic properties of InPd near-surface intermetallic phases obtained by annealing In thin films deposited on a polycrystalline Pd foil.[28] A stoichiometric InPd IMC exhibiting a "Cu-like" density of states could be formed by annealing a 4 monolayer equivalent (MLE) In film to 473 K. Catalytic characterization of this surface phase yielded a selectivity towards CO_2 of almost 100% between 493 and 550 K. Annealing led to a more In-diluted near-surface intermetallic phase exhibiting a more "Pd-like" density of states and an enhanced CO selectivity. In a previous study, we reported the formation of three rotational domains of a *bcc*-In_7Pd_3 compound with (110) orientation upon deposition of 4–35 MLEs of In metal on a Pd(111) substrate.[29] The film was characterized by x-ray photoemission spectroscopy (XPS), scanning tunneling microscopy (STM), and low-energy electron diffraction (LEED). This In-rich phase is metastable and transforms into a pure InPd(110) near-surface intermetallic phase between 500 and 600 K, depending on the initial coverage. This phase is also metastable and annealing above 600 K led to an In-depleted near surface region (~20 at. % In). Alloying effects have been studied by density functional theory (DFT) calculations by burying In-doped Pd layers in Pd(111).[30] The calculations demonstrated that In-doped Pd layers with In concentration below 50 at. % are energetically more favorable compared to In-rich layers. An In-rich layer would transform into a multilayer with lower In content in order to maximize the number of In-Pd bonds that are stronger than In-In and Pd-Pd bonds. This explains the metastability of 1:1 InPd surface phases on Pd(111) substrate and points toward the use of bulk InPd compounds as more realistic model systems.

A previous report by Franchy and Schmitz examined the InPd(111) single crystal surface under ultrahigh vacuum (UHV) conditions.[31] A clean surface was prepared by cycles of Ar^+ sputtering and annealing to 1070 K and produced a (1×1) LEED pattern of poor quality with broadened reflections, manifested by triangulated distortions of (h,k) spots and suggesting faceting. The surface was found very rough by STM. A $(2\sqrt{3} \times 2\sqrt{3})R30^\circ$ phase was observed by LEED and STM upon O_2 dosing at 750 K. No further details were given by the authors, in particular, regarding single crystal growth.

Here, we report a detailed study of the three low-index surfaces of the InPd compound using a combination of experimental methods (XPS, LEED, and STM). We show that different phases form depending on the surface preparation conditions. In addition, individual grains of a bulk polycrystalline sample are characterized by micro-spot XPS (μ-XPS), μ-LEED, and low energy electron microscopy (LEEM) techniques for comparisons. The results are interpreted in the light of DFT calculations of relative surface energies. We show that only one specific surface orientation — the (110) surface — contains active Pd atoms with a well-defined surrounding whereas the two other surfaces appear to be In terminated after annealing at temperatures close to the usual MSR reaction temperatures.

The paper is organized as follows. Experimental details are provided in Section II. The results are presented in Section III for the (100), (110), and (111) surfaces as well as for the bulk polycrystal. The main findings are discussed and summarized in Section IV.

II. EXPERIMENT

Single crystals were grown by the Czochralski method in Munich starting from an In-rich melt with composition $In_{62.5}Pd_{37.5}$ corresponding to a liquidus temperature of approximately 1373 K.[32] The pulling rate was reduced during the experiment from 0.20 down to 0.05 mm/h. The crystals were free of inclusions according to optical microscopy and scanning electron microscopy (SEM) investigations. The final bulk compositions of the single crystalline samples were in the range 52-54 at. % In, i.e., on the In-rich side of the composition window of InPd (38.5–55 at. % In).[33] The samples had a color similar to that of copper. Three different samples were extracted from these single crystals having their surface oriented perpendicular to either [100], [111], or [110] axis according to backreflection Laue X-ray diffraction. Each surface was mechanically polished using decreasing diamond grain sizes down to 0.25 μm followed by a final step with Syton OP-S, then successively rinsed in acetone and isopropanol. Clean surfaces were obtained

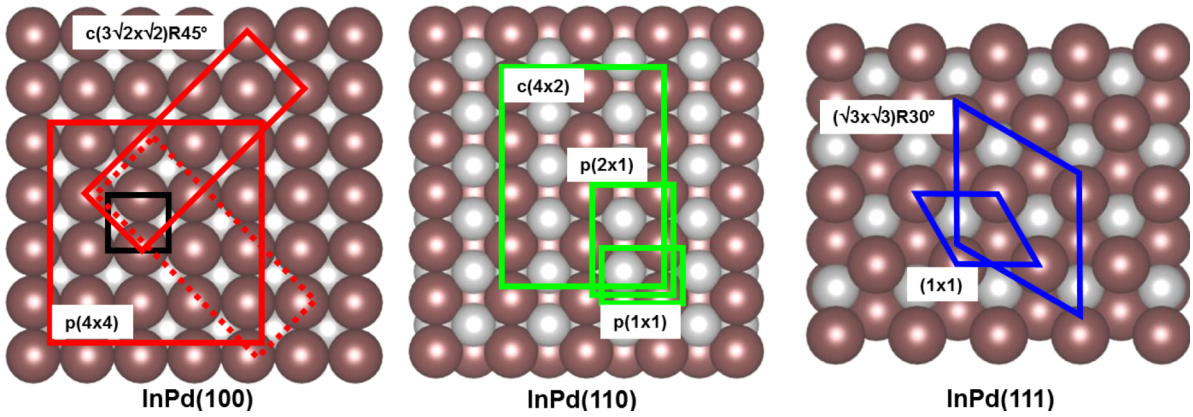

FIG. 1. Bulk terminated structure models of the three low-index surfaces of the InPd compound. The (100) and (111) surfaces terminate at either pure In or pure Pd planes whereas the (110) surface terminates at stoichiometric planes. The unit meshes of all surface reconstructions observed during surface preparation are drawn and labeled accordingly. They are slightly shifted from each other for clarity. An InPd(100)-(1×1) is shown for reference (not observed), represented by the small black square.

by sputter-annealing cycles (Ar^+, 1-2 kV). The annealing temperature was measured using an optical pyrometer with the emissivity set to 0.1. The temperature was also measured using a K-type thermocouple attached on the manipulator at some distance from the sample. There is a linear relationship between both measurements, with an offset of approximately 150° (thermocouple reading is lower than pyrometer reading). The surfaces were investigated under UHV conditions ($p \leq 2.10^{-10}$ mbar) using a multichamber system equipped with LEED, STM, XPS, and UPS.

In addition, a polycrystalline InPd sample with a nominal composition of $In_{47}Pd_{53}$ was synthesized in Nancy by induction melting under Ar atmosphere.[29] The ingot was further annealed in an evacuated quartz tube sealed under $He(90\%)/H_2(10\%)$ atmosphere (0.8 bar) up to 1248 K, maintained at this temperature for 36 h and then slowly cooled down to room temperature at a rate of 10 K/min. The structure was checked by powder X-ray diffraction (space group $Pm\bar{3}m$, CsCl type, $a = 3.23$ Å). The final composition as determined by energy dispersive x-ray analysis was $In_{47}Pd_{53}$, consistent with the existence domain of InPd.[33] The surface of the polycrystalline sample was prepared under UHV conditions by sputtering and annealing cycles (Ar^+, 1 keV, 973 K). The surface composition measured by XPS was $In_{53}Pd_{47}$, i.e., more In-rich than the bulk but within the compositional range of the InPd compound. The sample microstructure was analyzed by electron backscattered diffraction (EBSD) to determine the crystallographic orientation of the grains.

The polycrystalline sample was further investigated at beamline I06 of the Diamond Light Source (UK) using μXPS and LEEM techniques. Measurements were carried out using an Elmitec LEEM III and PEEM III (photoemission electron microscope).[34,35] The sample was probed with a linear polarized beam of monochromatic soft X-rays (μXPS) from the beamline (at a specified energy, between 80 and 2100 eV),[36] or a 15 keV electron beam (LEEM/LEED) which was retarded to a kinetic energy between 0 and 100 eV near the surface.

A dynamical LEED I(E) analysis was performed at Penn State University on the InPd(111) sample after cycles of Ar^+ sputtering (30 min. at 1 keV) and annealing to ~625 K. The sample was cooled to ~125 K and LEED patterns were recorded sequentially with increasing beam energy. The intensities from LEED (h,k) spots between 50 and 400 eV were extracted using the EasyLEED program[37] and compared to those of a theoretical model generated using the SATLEED code.[38] The agreement between the experiment and calculations was measured using the Pendry R-factor, and the statistical errors were calculated using the Pendry RR-function.[39] In the calculations, the scattering potential was described by 4 different sets of scattering phase shifts: two for the atoms near the surface (Pd/In) and the two other for the deeper layers (Pd/In). The relativistic phase shifts were calculated using the phase shift program that is packaged with the SATLEED code.[40] The relaxed parameters included the z-position of the top ten atoms, inner potential (real and imaginary part), the maximum value of angular momentum (l_{max}), and the Debye temperatures (208 K for In and 274 K for Pd). l_{max} was set to 8 at the beginning of the calculations and then increased until the best agreement was reached. The imaginary part of the inner potential was set to a fixed value at the beginning of the analysis (−4 eV), but in the final refinement, an energy dependent form $V_i = \text{constant} \times E^{\frac{1}{3}}$ was used. The total energy range for the dataset was 2700 eV and included 12 beams. The models tested included both ordered InPd compounds terminating at either pure Pd or In planes, and compounds with disordered alloy layers consisting of both Pd and In. The modeling of disordered alloy layers was achieved through application of the ATA (average T-matrix) approximation.[41]

III. RESULTS

A. Single crystal InPd surfaces: An overview

The bulk structure models of the three low-index surfaces of the InPd compound are illustrated in Fig. 1. The (100) and (111) surfaces can both terminate at either pure In or pure Pd planes. The distances between two consecutive geometric planes along [100] and [111] directions are 1.62 Å and 0.94 Å, respectively. The bulk terminated (110) surface

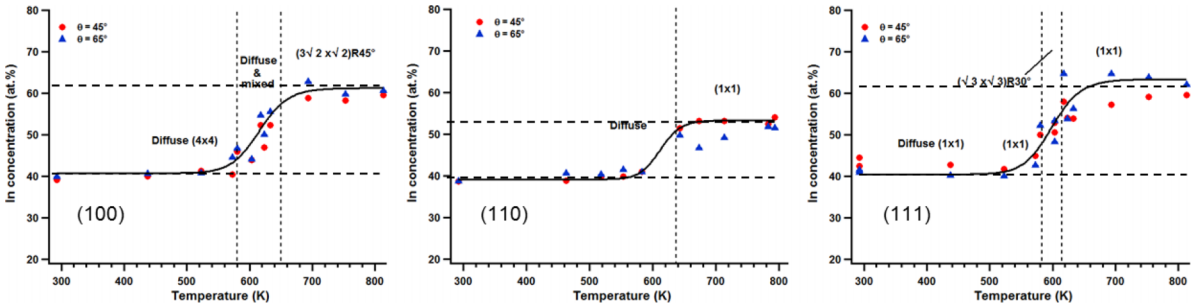

FIG. 2. Indium concentration in the near-surface region after sputtering (Ar^+, 2 keV for 30 min) and annealing as derived from XPS data for two different take-off angles θ. Solid lines in this figure are a guide for the eye. Vertical dotted lines indicate the temperature ranges for which the superstructures were observed. Horizontal dotted lines materialize the observed range of In concentration for the different surfaces. The first data points correspond to sputtered surfaces.

corresponds to stoichiometric planes separated by a distance of 2.30 Å.

The near-surface composition of the three samples has been monitored by XPS, for two different take-off angles, after sputtering and after annealing as a function of temperature. The results depicted in Fig. 2 show similar In depletion down to about 40 at. % In after sputtering, at all ion energies tested (1.0 keV, 1.5 keV, and 2.0 keV) and for the two take-off angles. All concentration measurements are given with an accuracy of ±5 at. %. We estimate below the information depth (ID) probed in XPS, which is defined as the sample thickness from which a specified percentage of the detected signal originates. It is given by $ID = -\lambda \times \cos\theta \times \ln [1\text{-}P/100]$, where λ is the inelastic mean free path of the photoelectrons, θ the emission angle of the photoelectrons with respect to the surface normal, and P a selected percentage.[42] The inelastic mean free path estimated using the analytical formula proposed by Tanuma *et al.* is about 1.2 nm for both In *3d* and Pd *3d* photoelectrons. It follows that 90% of the signal originates from a thickness of 1.95 nm at 45° take-off angle and 1.15 nm at 65°.[43] The near-surface composition after sputtering is thus homogeneous within the probed thicknesses and remains Pd-rich up to about 580 K. Above this temperature, the near-surface composition gradually evolves towards an In-rich composition on the order of ~60 at. % In for the (100) and (111) surfaces and ~55 at. % In for the (110) surface, i.e., on the In-rich side of the stoichiometric window or slightly above. The transition from a Pd-rich to an In-rich near-surface composition occurs within the same temperature window for the three surfaces. The temperature window within which the transition occurs is estimated between 580 and 660 K from the curves fitting the XPS concentration measurements shown in Fig. 2. Above 660 K, the composition remains approximately constant up to 800 K. Comparing measurements obtained for the two take-off angles suggest that the top surface is slightly more In-rich in the case of (100) and (111) surfaces whereas the subsurface of the (110) appears more Pd-rich than the top surface above 660 K.

These compositional changes in the near-surface region resulted in seven different superstructures as will be described below. The temperature range for which the superstructures were observed is mentioned in Fig. 2 and the theoretical unit cells of the superstructures over bulk truncated models of the three surfaces are depicted in Fig. 1.

B. The InPd(100) surface

Figure 3(a) shows a typical LEED pattern obtained after sputtering and annealing the (100) surface to 500 K and before the transition. The Pd-rich InPd surface appears as a quasi-ordered (4×4) superstructure as simulated in Fig. 3(b). The corresponding real space superstructure unit mesh is shown in Fig. 1. The LEED patterns are quite diffuse, indicating a poorly ordered surface. At this stage, the surface observed by STM is rather inhomogeneous with many areas characterized by step bunching and some area showing a terrace-and-step morphology. A unique step height of 3.25 ± 0.10 Å ~ a (the lattice parameter) is measured indicating that only one type of planes is selected as surface termination — potentially Pd planes according to XPS concentration measurements. A STM image of the quasi-ordered (4×4) superstructure is shown in Fig. 3(c). The random disorder of the prominent pseudo-square structures is obvious. The calculated fast-Fourier transform (FFT) shows a $p(4 \times 4)$ superstructure consistent

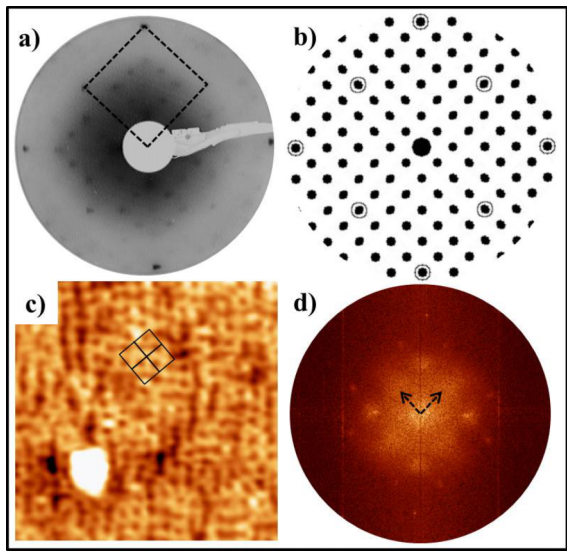

FIG. 3. (a) LEED pattern (50 eV) of the p(4×4) reconstruction on the InPd(100) surface. The (1×1) reciprocal space unit cell is shown as a dashed line. (b) Corresponding simulated LEED pattern. (c) STM image of the p(4×4) structure showing the quasi-ordered square structures (15 × 15 nm^2, +1.8 V, 0.09 nA). The black line indicates 4 reconstructed surface unit cells with dimensions 12.5 ± 0.50 Å ~ 4a. (d) Calculated FFT of a STM image. The dotted arrows indicate the lattice vectors of the reconstruction.

with the LEED patterns, with spots having non-homogeneous sharpness and intensity. Measurements from the FFT and 2D autocorrelation of STM images indicate an average surface lattice equal to 12.5 ± 0.50 Å ~ 4*a* for the p(4 × 4) unit cell (8.80 ± 0.50 Å for the pseudo-square structures).

Further annealing to temperatures between ~580 and 660 K leads to the coexistence of both a c($3\sqrt{2} \times \sqrt{2}$)R45° and the (4 × 4) superstructure. During this transitional state, LEED patterns are even more diffuse (not shown). These observations accompanied the transition from Pd-rich to In-rich InPd, so we could not correlate one particular superstructure to the stoichiometric composition $In_{50}Pd_{50}$. When annealing to temperatures corresponding to the upper plateau of Fig. 2, a sharp c($3\sqrt{2} \times \sqrt{2}$)R45° superstructure is observed by LEED as shown in Fig. 4(a) and depicted in the simulated pattern (Fig. 4(b)). Two domains coexist, which are rotated by 90° with respect to each other. This accounts for the four, rather than two, interior beams within the (1 × 1) reciprocal space unit cell. Calculated FFTs of the corresponding STM images reproduce the main features present in the LEED pattern (Fig. 4(d)). The rectangular unit cell dimensions are $a = 13.5 \pm 0.5$ Å and $b = 4.6 \pm 0.5$ Å, as measured by STM. The measured step heights of 3.30 ± 0.10 Å ≃ 2 × d_{100} suggest either In or Pd-terminated InPd(100), with potentially In planes as suggested by XPS concentration measurements. However, the fact that surface reconstructions are observed rather than a simple (1 × 1) termination, both below and above the transition, points towards a more complex chemistry of the top surface planes compared to simple Pd- or In-bulk truncated surfaces.

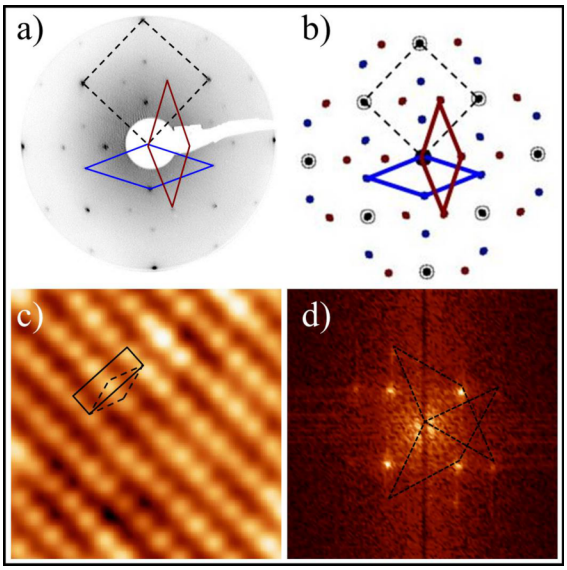

FIG. 4. (a) LEED pattern of the c($3\sqrt{2}\times\sqrt{2}$)R45° superstructure on InPd(100) surface recorded at a primary beam energy of 46 eV and (b) the corresponding simulated pattern. The InPd(100)-(1 × 1) square reciprocal unit cell (dashed line) and the primitive reciprocal unit cells of the c($3\sqrt{2}$ × $\sqrt{2}$)R45° (plain lines) are outlined. (c) STM image (5×5 nm^2, +1.4 V, 0.25 nA) of a single domain of the c($3\sqrt{2}\times\sqrt{2}$)R45° reconstruction. Both rectangular (solid line) and primitive (dashed line) unit cells are superimposed over the image. (d) Calculated FFT of a large scale STM image spanning the two rotational domains. The primitive reciprocal space unit cells from both domains are outlined (dashed lines).

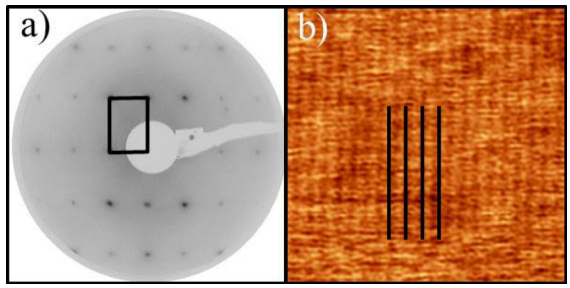

FIG. 5. (a) LEED pattern InPd(110)-(1 × 1) surface recorded at a primary beam energy of 140 eV acquired immediately after annealing at 640 K. (b) STM image of the surface showing atomic rows of either In or Pd atoms (9.4 × 9.4 nm^2, −1.5 V, 0.08 nA).

C. The InPd(110) surface

The LEED patterns of the InPd(110) surface remained diffuse up to the transition from a Pd-rich to a near stoichiometric surface. A good quality (1 × 1) LEED pattern was observed near the transition point at 640 K as shown in Fig. 5(a). This is consistent with the STM images recorded under the same preparation conditions showing atomic rows separated by a distance of 4.60 ± 0.50 Å (Fig. 5(b)) as expected for the rectangular unit cell of the InPd(110)-(1 × 1) surface. The atomic structure along the rows could not be resolved. The terrace step heights are measured at 2.30 ± 0.50 Å (not shown) and agree with the theoretical interlayer spacing (2.30 Å) of bulk truncated InPd(110). The (110) planes consist of alternating In and Pd atomic rows. The measured row spacing indicates that either In or Pd rows slightly protrude above the mean surface plane. The peak-to-peak roughness measured across line profiles in the direction perpendicular to the rows is in the order of 0.1 Å only.

Additional surface preparations involving higher annealing temperatures were also tested on the InPd(110) sample. In a first set of experiments, the sample was initially degassed to 980 K. This immediately led to a change in the visual appearance of the surface, from metallic mirror like to dull in luster. Next, a sputter-anneal (760 K) cycle followed by another (annealing to 620 K) was performed. After respective sputter-anneal cycles, (2 × 1) and (1 × 1) LEED patterns were observed (not shown). Only the (2 × 1) exhibited streaking, but both patterns showed extra diffraction spots characteristic of faceting (i.e., spots not converging towards the center (0,0) beam with increasing e-beam energy). Furthermore, composition measurements from XPS data indicated a near-surface composition close to the In-rich limit of the compositional range (55% In). At this stage, the sample was removed from the UHV system and characterized by optical microscopy as well as SEM. The dull appearance of the surface appeared to be due to the formation of faceted pits. Typical optical and SEM images of the faceted surface are shown in Fig. 6. All facets of the thermal etched pits can be explained by faces of the form {100} and {110} and there is almost no facet belonging to {111}. A sketch identifying each facets of a thermal etch pit is shown in Fig. 6. The lateral size of the pits was on the order of a few micrometers. At some different location on the sample, the pits had coalesced leading to an even rougher surface.

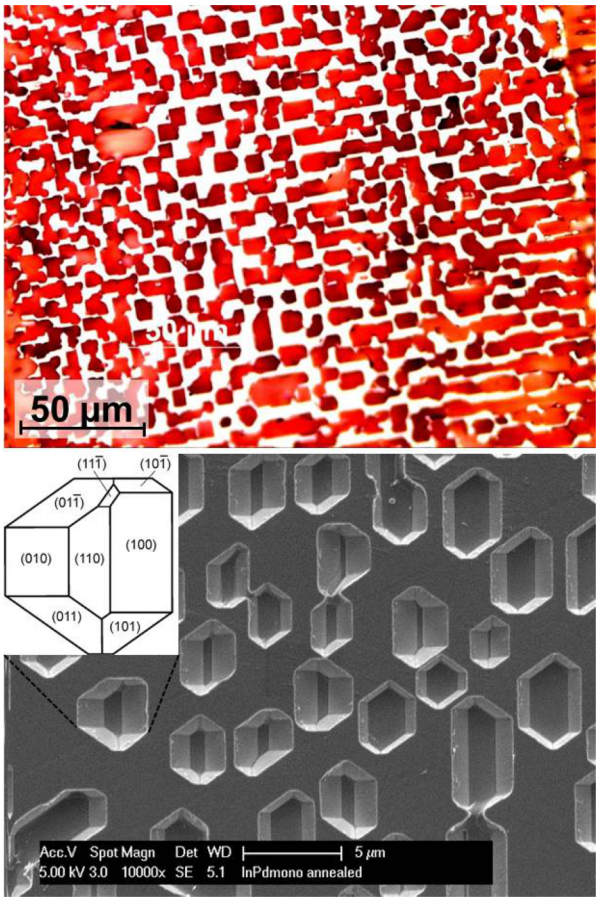

FIG. 6. Optical image in false color (top) and SEM image (bottom) of the faceted InPd(110) surface obtained after annealing at 980 K. The two images correspond to different surface regions. The red parts in the top image are holes in the surface. The inset in the bottom image shows a sketch identifying each facets of a thermal etch pit.

After this set of experiments, the sample was re-polished before further UHV studies. Then, the sample was initially degassed at 470 K followed by several sputter-anneal cycles, increasing the annealing temperature by 50 K over the course of one or two cycles. A diffuse (1×1) LEED pattern was first observed up 625 K (not shown), which improved in quality until a $c(4 \times 2)$ reconstruction was observed near 675 K (Fig. 7(a)). Annealing to 735 K led to a weak (2×1) LEED pattern. The (2×1) reconstruction could be observed up to 875 K which eventually led to the formation of facets again. Once faceting occurred, an InPd(110)-$c(4 \times 2)$ pattern could not be reproduced by the same sputtering and annealing conditions (i.e., 675 K). The (2×1) LEED pattern is shown in Fig. 7(b). The formation of these two surface reconstructions was correlated with an increase in the In near-surface concentration (see Fig. 8), well above the saturation plateau previously observed in Fig. 2(b). STM images acquired on both the $c(4 \times 2)$ and (2×1) reconstructions indicated a rather rough surface with wedding cake structures and no large flat terraces. It was therefore not possible to obtain atomically resolved STM images of these two surface phases.

Upon further annealing to 970 K and up to 1170 K, the surface became dull again due to the formation of macroscopic facets, consistent with the previous set of experiments. The LEED pattern evolved from a diffuse $p(2 \times 1)$ pattern to a sharp (1×1) (see Fig. 7(c)), with clear evidence of faceting in the LEED movies (see Fig. S1 of the supplementary material showing a LEED movie of the InPd(110) surface after annealing at 970 K[44]). Medium size terraces could only be observed by STM for the InPd(110)-(1×1). Accurate step-height measurements gave a value of 2.29 ± 0.05 Å corresponding to the interplanar distance d_{110}. The structure on terraces revealed atomic rows with an average row spacing of 4.60 ± 0.10 Å meaning that either Pd or In atomic rows slightly protrude above the mean plane position, similar to the low-temperature InPd(110)-(1×1) phase previously discussed (Fig. 5(b)). The structure along the rows could not be resolved. The near-surface composition measured by XPS after annealing at 1170 K was $In_{52.0\pm5.0}Pd_{48.0\pm5.0}$ and was found homogeneous between the surface and subsurface layer within error. Therefore, XPS, STM, and LEED results pointed towards a bulk-truncated InPd(110) stoichiometric surface. Within this (buckled) plane, Pd atoms have a well-defined and similar surrounding of In atoms and Pd atoms. Furthermore, these atomic ensembles are stable upon high temperature annealing (1170 K), i.e., there is no obvious surface segregation tendency.

D. The InPd(111) surface

The InPd(111) surface was investigated by XPS, LEED, STM, and dynamical LEED I(E). XPS data showed a similar

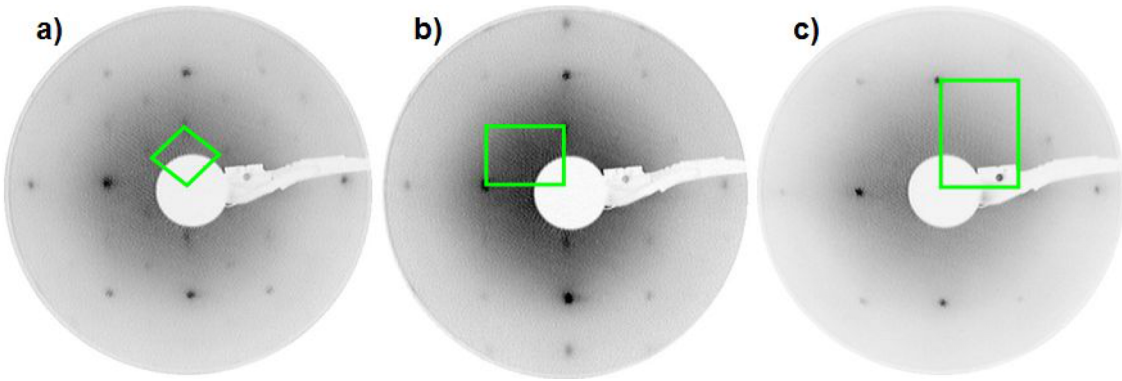

FIG. 7. LEED patterns of the (a) $c(4\times2)$, (b) (2×1), and (c) (1×1) phases observed on the InPd(110) surface, recorded at the same electron beam energy of 63 eV. The primitive reciprocal space unit cells for each surface phase are also shown (green solid line).

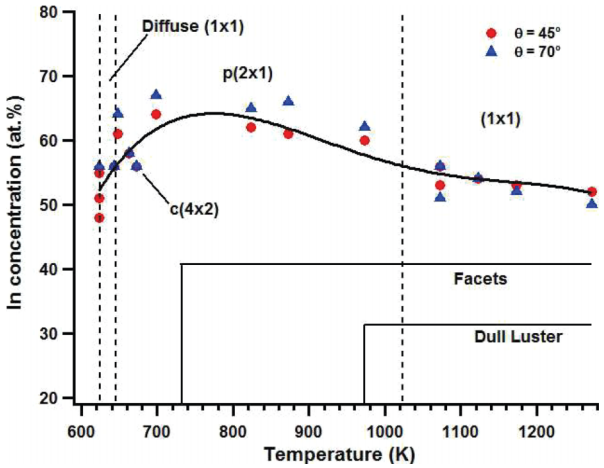

FIG. 8. Surface compositions and LEED observations from the second set of InPd(110) experiments are displayed above. Each measurement/observation was performed after sputtering and annealing the surface. The windows labeled "facets" and "dull luster" represent the respective annealing temperature range where initial faceting and change in the surface appearance can be expected. However once facets start to appear, they can hardly be removed by sputtering. Also the "dull luster" is irreversible until the sample is re-polished.

trend to that of InPd(100), with a transition from a Pd-rich to an In-rich near-surface composition between 580 and 660 K (Fig. 2(c)). A (1×1) structure was predominantly observed by LEED both before and after the transition (Fig. 9(a)). During the transition, a $(\sqrt{3} \times \sqrt{3})R30^\circ$ superstructure was also observed (Fig. 9(b)). However, it existed as the primary structure within a very narrow composition window around stoichiometry. Note that the boundary-lines of Fig. 2(c) correspond to observations of weak $(\sqrt{3} \times \sqrt{3})R30^\circ$ LEED patterns.

A STM image of the $(\sqrt{3} \times \sqrt{3})R30^\circ$ phase together with its corresponding FFT is shown in Figs. 9(c) and 9(d). The unit

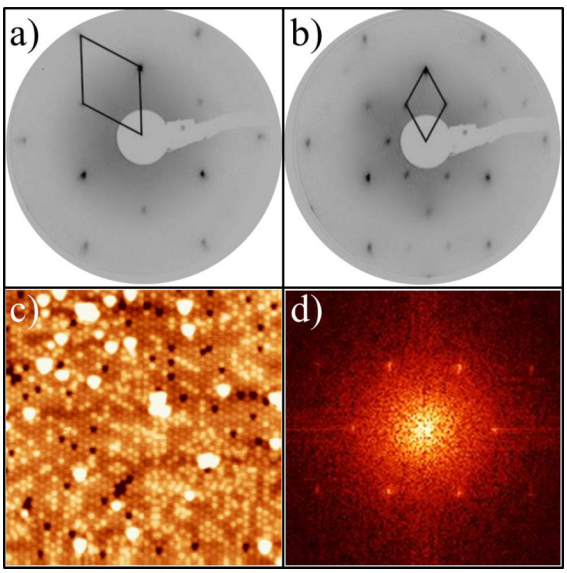

FIG. 9. LEED images, both taken at 50 eV primary beam energy, showing (a) the (1×1) phase and (b) the $(\sqrt{3} \times \sqrt{3})R30^\circ$ superstructure on the InPd(111) surface. The reciprocal unit cells are shown as solid lines. (c) STM image (30×30 nm^2, +1.8 V, 0.09 nA) of the InPd(111)-$(\sqrt{3} \times \sqrt{3})R30^\circ$ phase and (d) corresponding FFT.

mesh has a lattice constant $a = 7.90 \pm 0.10$ Å, in agreement with expected theoretical values (Fig. 1). The measured step height is 1.85 ± 0.05 Å, suggesting a preferred In or Pd termination ($2 \times d_{111} = 1.876$ Å). An identical step-height was measured for the InPd(111)-(1×1) phase. The composition of the In-rich phase showed a slight enrichment of In ($\lesssim$5%) in the top few layers, but within error of In-rich InPd(111). This may be attributed to a preferred In termination after the transition. For the InPd(111)-$(\sqrt{3} \times \sqrt{3})R30^\circ$ structure, the composition was near $In_{50}Pd_{50}$ and uniform between top layers (1-3) and sublayers (3-5). STM images show atomic protrusions having two different kinds of contrasts representing an height difference of 0.3 Å (Fig. 9(c)). In addition, holes and protrusions with dark and white contrast, respectively, are also observed. They are 0.8 Å below or above the mean surface plane. The STM contrast showed negligible dependence on the tip bias, which was varied in 0.2 V increments from −1.4 to +1.4 V. Therefore, we cannot rule out a true topographical effect. Note that the atomic radii difference of In and Pd is only 0.15 Å,[45] which is smaller than the surface roughness. The STM contrast suggests a chemically mixed surface plane, with no long-range chemical ordering as judged from the distribution of bright and dim protrusions. This is consistent with the XPS composition measurements. The dark holes and white protrusions may be influenced by the subsurface defects. The $(\sqrt{3} \times \sqrt{3})R30^\circ$ phase seems to be a transient state which can only be frozen in between the transition from the Pd-rich to the In-rich terminated (1×1) surface.

A LEED I(E) structure analysis was performed for the Pd-rich InPd(111)-(1×1) surface. Several models were tested, including disordered alloys (with In:Pd 50:50 mixture in both top and top two layers) and ordered alloys terminating at either In or Pd bulk planes for a total of 4 combinations. Initial agreement evaluated using the Pendry R-factor for disordered alloys ($\geq$0.60) was worse than for other models. So we can rule out a 50:50 mixed terminated surface as was determined by LEED I(E) analysis on NiAl(111), another CsCl-type compound.[46] Furthermore, seven other ordered structures (corresponding to pure In or Pd terminations) were tested. Terminations of the top four layers differed as such: In-Pd-In-Pd, Pd-In-In-Pd, In-Pd-Pd-In, In-Pd-In-In, Pd-In-Pd-Pd, Pd-Pd-In-Pd, In-In-Pd-In. The fifth layer had the opposite termination as the fourth layer and lower planes alternated as expected for bulk InPd(111). The best overall Pendry R-factor was 0.26 for simple ordered InPd, with Pd on the top layer. Both experimental and theoretical I(E) curves for 12 separate beams of the Pd-rich InPd(111)-(1×1) structure are shown in Fig. 10. The optimized structure (Fig. 11) showed a substantial outward expansion of the top and third layer. The second and fourth layers contracted into the bulk (bulk interplanar distance: 0.9379 Å). These parameters, along with all interplanar spacings for the top 10 layers, are shown in Table I. The LEED I(E) analysis of the low temperature InPd(111) phase and the XPS results are consistent with a bulk-terminated surface at pure Pd plane. Though a similar LEED I(E) analysis is not available for the high temperature phase, XPS and STM data suggest a bulk-terminated at pure In plane. Therefore, only in the transition regime does the

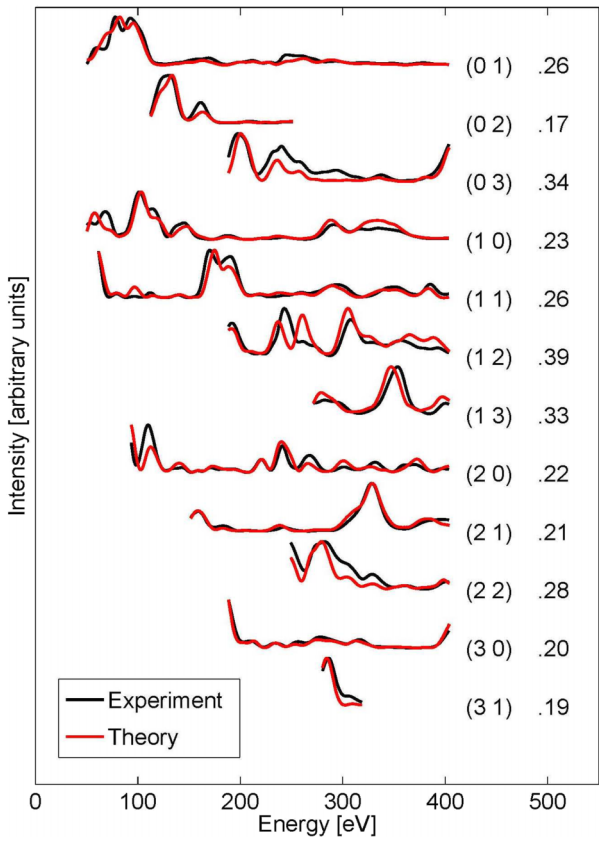

FIG. 10. The experimental vs. theoretical I(E) curves for 12 separate beams of the Pd-rich InPd(111)-(1 × 1) structure are shown. The theoretical data are from the best-fitted model of Fig. 11 and Table I. Individual R factors for each (h, k) beam are indicated next to respective plots. A total R factor of 0.26 were calculated from the entire data set (total range of 2700 eV).

InPd(111) surface presents a bimetallic chemistry which is metastable. Thus, the (111) surface is expected to be of less interest for catalysis.

E. Polycrystalline InPd

After several sputtering and annealing cycles under UHV, macroscopic grains could be observed optically at the surface of the polycrystalline sample as shown in Fig. 12. The sample had a circular shape with a diameter of about 10 mm. The average lateral grain size is rather large, on the order of several hundreds of μm and up to 1 mm. The microstructure of the

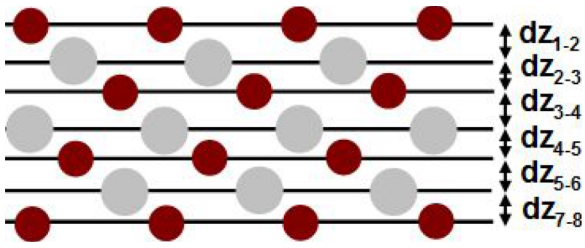

FIG. 11. The above profile of the Pd-rich InPd(111)-(1 × 1) surface, viewed along the [$\bar{1}$ 0 1] axis, illustrates interlayer spacings in accordance with values of Table I. The expansions/contractions of planes are slightly exaggerated for clarity. Pd (In respectively) atoms are represented as red (grey respectively) circles.

TABLE I. Interlayer spacing (dz_{a-b}) (Å). The bulk interplanar distance: 0.9379 Å.

Interlayer spacing (dz_{a-b}) (Å)
$dz_{1-2} = 1.01 \pm 0.02$
$dz_{2-3} = 0.82 \pm 0.02$
$dz_{3-4} = 1.07 \pm 0.02$
$dz_{4-5} = 0.89 \pm 0.02$
$dz_{5-6} = 0.95 \pm 0.02$
$dz_{6-7} = 0.92 \pm 0.03$
$dz_{7-8} = 0.93 \pm 0.03$
$dz_{8-9} = 0.96 \pm 0.03$
$dz_{9-10} = 0.88 \pm 0.04$
$dz_{10-bk} = 0.97 \pm 0.05$

polycrystalline sample was investigated *ex situ* using EBSD, allowing the determination of crystallographic orientation of each grain deduced from the Kikuchi pattern. The EBSD map shown in Fig. 12 indicates that the grains observed optically correspond to individual grains having a single orientation and the pole figures show the absence of preferred orientation of the grains, i.e., no texture.

The surface of the polycrystal was further studied at beamline I06 of the Diamond Light Source (UK) using LEEM, μXPS, and micro-spot LEED. In this case, the surface was prepared by Ar^+ sputtering and annealing cycles in a temperature range of 875–935 K. Some examples of LEEM images and micro-spot LEED patterns recorded are shown in Fig. 13. Note that the field of view (FOV) typically used in LEEM is much smaller than the average grain size for this sample. Figs. 13(a) and 13(b) show grain boundaries separating relatively smooth grains (SG1 and SG2) from rougher grains (RGs). The smooth grains are not perfectly flat either and SG1 is clearly rougher than SG2, for example, as can be seen from Figs. 13(c) and 13(d). From the EBSD

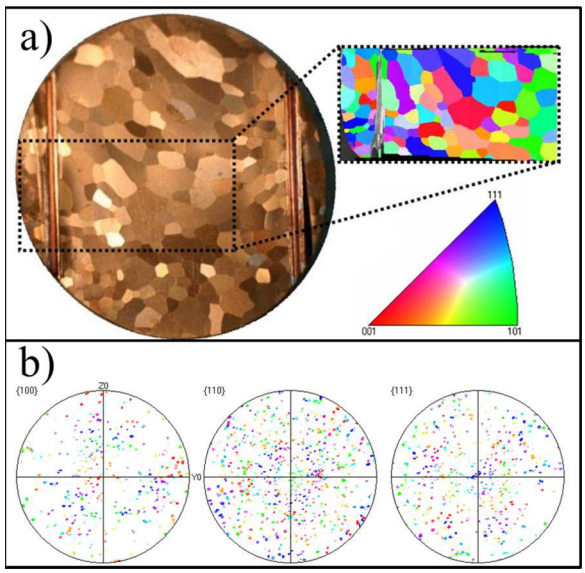

FIG. 12. (a) Picture of the polycrystalline InPd sample (left) image and EBSD map acquired in the sampled area shown by the dotted rectangle (right). The orientation triangle indicates the color code of the grains. (b) Pole figures obtained from the EBSD map indicate the absence of texture.

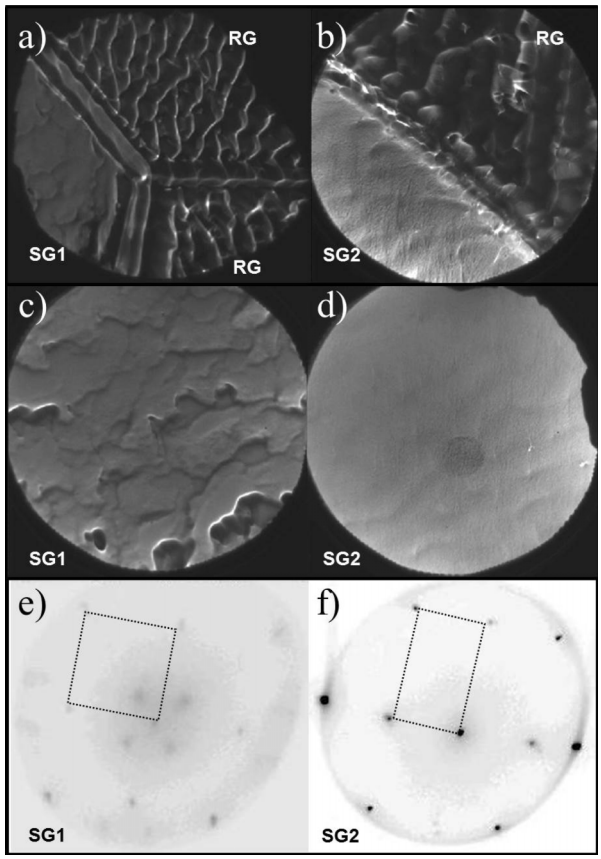

FIG. 13. ((a) and (b)) LEEM images of smooth grains SG1 and SG2 surrounded by rough grains, RG. The field of view (FOV) is 80 μm in (a) and 30 μm in (b). ((c) and (d)) LEEM images of SG1 and SG2 (both with 50 μm FOV). (e) Micro-spot LEED pattern from SG1 recorded at 29 eV showing a diffuse square pattern with additional interior spots consistent with a (100)-(4×4) reconstruction. (f) Micro-spot LEED pattern from SG2 recorded at 30 eV consistent with a well-ordered (110)-(1×1) surface structure.

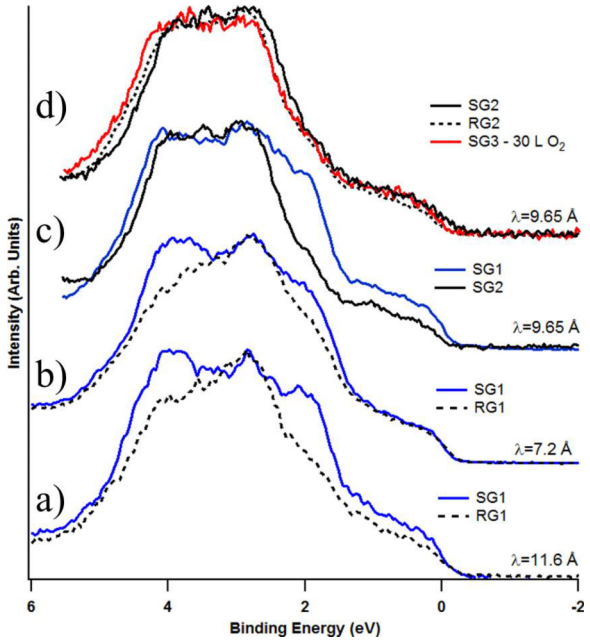

FIG. 14. ((a) and (b)) VB spectra from SG1 and RG1 for two different probing depths. The inelastic mean free path λ displayed next to the graph was approximated using the kinetic energies around 643.5 eV (a) and 245.5 eV (b). (c) VB spectra from SG1 and SG2 showing substantial difference in the DOS. (d) VB spectra from SG2 and RG2. The stop voltage was 445.5 eV. Another smooth grain (SG3) shows similar VB spectrum despite a small but measurable amount of surface oxygen after the surface had been exposed to 30 L of O_2.

results, it may be speculated that the grain roughness is linked to the misorientation of its average surface with respect to one of the high symmetry directions. This accounted, in part, for a more diffuse LEED pattern for SG1 than for SG2 (Figs. 13(e) and 13(f)). The LEED pattern of SG1 points indicates a square lattice with some additional diffuse spots within the unit cell pointing towards a large surface structure. Although the LEED pattern is distorted, it seems consistent with the (100)-(4 × 4) reconstruction reported earlier for the (100) single crystal surface annealed at low temperature. The c($3\sqrt{2} \times \sqrt{2}$)R45° phase is expected at high annealing temperature. The sharp LEED pattern from SG2 indicates a (110)-(1 × 1) surface structure, as expected from the (110) single crystal study. It was also found that the SG2 LEED pattern remained unchanged after either 30 L O_2 or 20 L of H_2 surface exposure at room temperature.

The chemical composition of individual grains was measured by μXPS and was found to correspond to the In-rich InPd phase. Some small variations among the grains could be observed. For example, the In content of SG2 was slightly less than that of other grains measured. This is consistent with a (110) surface orientation for which the near-surface In concentration is expected to be lower than for other low-index surfaces as previously discussed. Some traces of oxygen could also be observed at grain boundary regions (global composition: $In_{59}Pd_{37}O_4$). Oxygen trapped at grain boundaries might also induce some In-enrichment as well.

The valence band (VB) was measured by μXPS for several grains and for different stop voltages in order to vary the surface sensitivity of the measurements. The results are illustrated in Fig. 14 where all spectra have been normalized to their maximum. The VB is dominated by the Pd 4*d* band that spreads between 1.5 and 5 eV below the Fermi level. No obvious change can be seen when the surface sensitivity is varied as shown for SG1 and RG1 (Figs. 14(a) and 14(b)). The most noticeable difference between all these spectra concerns the relative intensity of the feature at approximately 2 eV below the Fermi level, which is higher for SG1 compared to SG2 (Fig.14(c)). Because SG1 and SG2 have been identified as (110) and (100) grains, respectively, this change in the surface electronic density of states might be linked to the presence of Pd surface atoms in (110) planes compared to (100) surface planes. Note that the VB structure does not seem to be significantly modified after exposing the surface to 30 L of O_2 (Fig. 14(d)).

A separate set of concentration measurements were performed using in-house XPS equipped with a Mg K_α source (1253.6 eV) and an analyzer aperture setting for a lateral sampling area of ~1.6 mm, thus averaging over several grains. We found a global composition of $In_{53}Pd_{47}$, which was the same as the average value obtained from SG and RG measurements. Some additional STM measurements were performed on few grains. Most grains appeared rough as a result of step bunching, most likely because of their

misorientation with respect to a low-index plane. A few grains revealed a terrace and step morphology, with a terrace size on the order of several tens of nm and a STM contrast similar to that of the InPd(100)-p(4 × 4) shown in Fig. 3(d). The limited number of sampled grains did not allow to observe other structures in this set of experiments.

IV. DISCUSSION AND CONCLUSIONS

The three low-index surfaces ((100), (110), and (111)) of an InPd single crystal have been investigated under UHV conditions as a function of the annealing temperature. All three surfaces showed a transition from an In-depleted near-surface composition induced by preferential sputtering to an In-rich near surface composition upon annealing. The transition occurred in a temperature range between 580 and 660 K. The In concentration in the In-rich limit of the transition was higher for the (100) and (111) surfaces (~60 at. %) than for the (110) surface (~55 at. %). These concentration differences in the In-rich limit are interpreted as a consequence of surface plane selection at pure In bulk planes in the case of (100) and (111) surfaces while the (110) surface terminates at stoichiometric planes. Several surface reconstructions have been identified. On the (100) surface, a pseudo-square structure was observed at low temperature (diffuse (4 × 4) phase) evolving into a sharp c($3\sqrt{2} \times \sqrt{2}$)R45° superstructure above the transition temperature. The pseudo-square was also observed on individual grains of the polycrystalline sample after annealing at higher temperature (970 K). On the (111) face, the surface evolves from a Pd-terminated (1 × 1) surface according to the LEED-I(E) analysis below the transition to an In-rich (1 × 1) surface above the transition temperature. A chemically disordered ($\sqrt{3} \times \sqrt{3}$)R30° superstructure is also observed during the transition. The (110) face is mainly disordered below the transition and shows a (1 × 1) pattern above the transition. Annealing further to higher temperatures leads to the formation of other superstructures (c(4 × 2), p(2 × 1), (1 × 1)) but also to the formation of macroscopic faceted pits. Despite the formation of these faceted holes, the (110) surface remains stoichiometric and is the only low-index surface containing well-separated Pd sites surrounded by In atoms. We already mentioned that the (110) termination is buckled, indicating that either In or Pd rows protrude slightly above the mean surface plane.

Previously, we reported DFT calculations predicting which of the In or Pd atomic rows should protrude at the (110) surface.[30] The surface energy of the non-relaxed (110) surface was evaluated by a linear regression on the total energy of different symmetric slabs built with an increasing number of planes, leading to $\gamma_{(110)}^{non-relaxed} = 0.82$ J/m^2. A similar calculation was performed on an asymmetric slab to determine the surface energy of the relaxed (110) surface, leading to $\gamma_{(110)}^{relaxed} = 0.72$ J/m^2. The significant relaxation energy of the (110) surface (0.10 J/m^2) was attributed to atomic relaxation within the surface plane: the Pd atoms move slightly below the surface plane while the In atoms move slightly above, resulting in a height difference of 0.26 Å between the two species. This is consistent with the fact that only one type of atomic rows is imaged by STM on the InPd(110) surface. A similar observation was also reported for the InPd(110) near-surface intermetallic phase formed by annealing In thin films deposited on a Pd(111) substrate.[29] The fact that In atoms slightly protrude above the mean surface plane can be rationalized by the smaller elemental surface energy of In compared to Pd ($\gamma_{In(001)}^{bct} = 0.675$ J/m^2; $\gamma_{Pd(111)}^{fcc} = 2.05$ J/m^2). Calculations of the In segregation energy at the perfect InPd(110) surface showed that In segregation is unfavorable, due to the relatively large energy required to break In-Pd bonds, while In antisites tend to segregate to the surface in off-stoichiometric InPd(110) systems.[30] Again, this is consistent with experimental observations showing a (nearly) stoichiometric concentration for the (110) near surface concentration after annealing above the transition. This result is also supported by recent quantum chemical calculations showing that the crystal structure of InPd is stabilized by ionic and multi-center In-Pd interactions.[47] The c(4 × 2) and p(2 × 1) superstructures observed at higher annealing temperatures (700 to 800 K) coincide with a temporary In enrichment of the surface (Fig. 8). A (1 × 1) pattern is recovered above 800 K and faceting occurs simultaneously while the near surface concentration returns to stoichiometry. The faceting of InPd single crystals upon long-term high-temperature annealing was also observed and studied in detail by Hahne.[48] Electron probe microanalysis (EPMA) of the concentration profile perpendicular to the crystal growth direction revealed a small decrease in the In content from the center to the rim of the crystal, on the order of 1 at. %. This was attributed to In evaporation from the surface during ongoing growth, due to the high vapor pressure of In compared to Pd metal. The bulk compositions of the single crystal samples were in the range 52-54 at. % In. The constitutional defects have been determined and are Pd vacancies for In-rich compositions and Pd antisites for Pd-rich compositions.[49] Vacancy condensation at the surface might thus be an additional mechanism for the formation of the faceted holes. This implies a significant mobility in this temperature regime. In a similar temperature regime (723 K) and under reactive atmosphere (presence of methanol and water), experiments on a polycrystalline In-Pd sample have shown that indium segregates to the surface forming In_2O_3.[50] The stability of InPd bimetallic particles under oxidation conditions has also been tested and it was shown that the particles fully decompose into Pd and In_2O_3 already at 573 K.[51]

To further understand the trends observed experimentally for the (100) and (111) surfaces, we have performed additional calculations not reported previously. The surface energies of the non-stoichiometric (100) and (111) surfaces have been evaluated by DFT calculations. The method and the parameters linked to the numerical implementation of the DFT calculations are the same as those described by Gaudry *et al.*[30] In the case of non-stoichiometric surfaces like InPd(100) and (111), the compositions of the bulk and the slab differ. When dealing with a symmetric slab, consisting of N_{In} In atoms and N_{Pd} Pd atoms, the surface energy γ is given by

$$\gamma = \frac{1}{2A}(E_{slab}(N_{In}, N_{Pd}) - N_{In}\mu_{In} - N_{Pd}\mu_{Pd}), \qquad (1)$$

where μ_{In} (respectively μ_{Pd}) is the chemical potential of the In atom (resptively Pd atom) in the slab. This equation is valid

TABLE II. Surface energies (J/m^2) of low-index surfaces of InPd. $A_{(hk\ell)}$ is the surface area of the (hkl) surface (Å ^{2}).

	(110)	$(100)^{Pd}$	$(100)^{In}$	$(111)^{Pd}$	$(111)^{In}$
	$A_{(110)} = 15.40$	$A_{(100)} = 10.89$		$A_{(111)} = 18.87$	
Pd-rich	0.72	0.93	1.40	0.70	1.10
In-rich	0.72	1.68	0.65	1.14	0.67

only if the atoms are not exchanged between the bulk and the surface, an assumption which is not justified experimentally. The exact surface composition is not known precisely either, as it depends on the experimental surface preparation conditions for instance, making it difficult to predict the preferred surface termination in such cases. Nevertheless a common approach is to assume that the variations in the surface preparation conditions may be represented by deviations of the actual chemical potential from the bulk values. This is the approach developed in a large number of studies and is applied for the (100) and the (111) surfaces in the following.[52–54]

The (100) and (111) surfaces are terminated either by Pd atoms ($(100)^{Pd}$ and $(111)^{Pd}$) or by In atoms ($(100)^{In}$ and $(111)^{In}$). For each low-index surface, we have determined the surface energies of the two possible terminations, as a function of the In chemical potential, using symmetric slabs. A 13-layer thick slab has been used for the InPd(100) surface and a 19-layer thick slab for the InPd(111) surface because relaxations are larger in this latter case.

In Table II, surface energies are given in the In-rich limit ($\mu_{In} = \mu_{In}^{bulk} = -2.35$ eV) and in the Pd-rich limit ($\mu_{In} = \mu_{In}^{bulk} - \Delta H_f^{InPd} = -3.37$ eV). The calculated surface energy of the (110) surface is also recalled.

From Table II, it appears that the (110) surface presents a lower energy compared to the average values for (111) and (100) surfaces terminated at either Pd or In atoms. This might be due to the lower atomic surface density of (111) and (100) surfaces compared to the (110) surface. The surface energy anisotropies $\frac{\gamma_{(111)}}{\gamma_{(110)}}$ and $\frac{\gamma_{(100)}}{\gamma_{(110)}}$ are calculated to be 1.25 and 1.62, respectively, in acceptable agreement with the values predicted from the broken bond model ($\frac{\gamma_{(111)}}{\gamma_{(110)}} = \sqrt{\frac{3}{2}}$ and $\frac{\gamma_{(100)}}{\gamma_{(110)}} = \sqrt{2}$). It means that the surface energy of the InPd intermetallic compound is predominantly determined by the first neighbors (In-Pd bonds). The discrepancy between the values given by the broken-bond model and the calculated ones may come from contributions of the farther neighbors. In addition, it is well known that the generalized-gradient approximation (GGA) underestimates absolute surface energies,[55] while correctly predicting relative surface energies in most cases.[56]

The calculated energies suggest a Pd-termination (respectively In-termination) for Pd-rich (respectively In-rich) alloy compositions, for both the (100) and (111) surfaces. These conclusions are supported by the LEED-I(E) analysis of the Pd-rich InPd(111) surface prepared at low annealing temperature (before the transition), which points towards a bulk-terminated surface at Pd-plane. In the In-rich limit, LEED and XPS data for the (111) surface are also consistent with bulk-terminated surface at In plane. In the case of the (100) surface, a more complex surface reconstruction is observed which is not considered in the calculations. The structures of the low-indexed surfaces of the InPd compound appear to be less ordered than those of the related GaPd system with B20 structure, which is almost a line compound.[24,26,57] This may be related to higher degree of covalency of the bonding in GaPd compared to InPd.

Finally, in our previous work on In thin films deposited on Pd substrates, we have shown that a 1:1 InPd near surface intermetallic phase forms upon annealing between 500 and 600 K, depending on the initial coverage.[29] The thermal stability of such model system is however limited and the In concentration in the near-surface region decreases to about 20 at. % above 600 K. Therefore, single crystal surfaces should be considered as better model systems for further studies of their surface reactivity. We also found that grains from a polycrystalline sample observed individually reproduced the behavior expected from single crystal studies, thus providing a trustful average of all low index orientations although far less convenient for comprehensive surface studies. The μXPS VB spectra recorded on individual grains suggested small variations of the density of states within 2 eV below the Fermi level depending on the orientation of the grains. Although small changes in d-band center and width can be correlated with drastic changes in the catalytic properties as shown in the case of polycrystalline ZnPd,[23] our structural analysis of the different low-index InPd surfaces clearly shows that only specific surface orientations contain Pd atoms with a well-defined surrounding of In and Pd atoms, i.e., the (110) surface in this case. The (110) surface is thus expected to be the most active for MSR reaction compared to the (100) and (111) In-terminated surfaces. A perspective of this work would be to perform MSR catalytic characterization on the three separate single crystal surfaces to correlate properties with surface structures. In addition, the surface structures of real catalysts under MSR conditions may not be the same as those of surfaces prepared under UHV conditions, due to indium oxide formation. It would thus be interesting to study further the stability of the different InPd surfaces under oxidation conditions and the formation of surface oxides.

ACKNOWLEDGMENTS

This work was supported by the joint ANR-DFG CAPRICE No. 2011-INTB 1001-01, the European C-MAC consortium, and COST Action CM0904 "Intermetallic compounds as catalysts for steam reforming of methanol (IMC-SRM)" and CNRS (INCAS Project No. PICS05892). This work was granted access to the HPC resources of IDRIS under the Allocation No. 2015096339.

[1]D. L. Trimm and Z. I. Önsan, Catal. Rev. **43**, 31 (2001).
[2]G. A. Olah, Angew. Chem., Int. Ed. **44**, 2636 (2005).
[3]D. R. Palo, R. A. Dagle, and J. D. Holladay, Chem. Rev. **107**, 3992 (2007).
[4]X. Cheng, Z. Shi, N. Glass, L. Zhang, J. Zhang, D. Song, Z.-S. Liu, H. Wang, and J. Shen, J. Power Sources **165**, 739 (2007).
[5]S. Sa, H. Silva, L. Brandao, J. M. Sousa, and A. Mendes, Appl. Catal., B **99**, 43 (2010).
[6]W. Stadlmayr, C. Rameshan, C. Weilach, H. Lorenz, M. Hävecker, R. Blume, T. Rocha, D. Teschner, A. Knop-Gericke, D. Zemlyanov, S. Penner, R. Schlögl, G. Rupprechter, B. Kloetzer, and N. Memmel, J. Phys. Chem. C **114**, 10850 (2010).

[7]M. Armbrüster, M. Behrens, K. Föttinger, M. Friedrich, E. Gaudry, S. K. Matam, and H. R. Sharma, Catal. Rev.: Sci. Eng. **55**, 289 (2013).
[8]N. Iwasa, S. Kudo, H. Takahashi, S. Masuda, and N. Takezawa, Catal. Lett. **19**, 211 (1993).
[9]N. Iwasa, S. Masuda, N. Ogawa, and N. Takezawa, Appl. Catal., A **125**, 145 (1995).
[10]N. Iwasa and N. Takezawa, Top. Catal. **22**, 215 (2003).
[11]W. M. H. Sachtler, Catal. Rev.: Sci. Eng. **14**, 193 (1976).
[12]K. Kovnir, M. Armbrüster, D. Teschner, T. V. Venkov, F. C. Jentoft, A. Knop-Gericke, Y. Grin, and R. Schlögl, Sci. Technol. Adv. Mater. **8**, 420 (2007).
[13]M. Armbrüster, K. Kovnir, Yu. Grin, and R. Schlögl, *Complex Metallic Alloys: Fundamentals and Applications*, edited by J. M. Dubois and E. Belin-Ferré (Wiley-VCH, Weinheim, 2011).
[14]A. P. Tsai, S. Kameoka, and Y. Ishii, J. Phys. Soc. Jpn. **73**, 3270 (2004).
[15]A. Bayer, K. Flechtner, R. Denecke, H. P. Steinrück, K. M. Neyman, and N. Rösch, Surf. Sci. **600**, 78 (2006).
[16]K. M. Neyman, K. H. Lim, Z.-X. Chen, L. V. Moskaleva, A. Bayer, A. Reindl, D. Borgmann, R. Denecke, H.-P. Steinrück, and N. Rösch, Phys. Chem. Chem. Phys. **9**, 3470 (2007).
[17]G. Weirum, M. Kratzer, H. P. Koch, A. Tamtögl, J. Killmann, I. Bako, A. Winkler, S. Surnev, F. P. Netzer, and R. Schennach, J. Phys. Chem. C **113**, 9788 (2009).
[18]C. Rameshan, W. Stadlmayr, C. Weilach, S. Penner, H. Lorenz, M. Hävecker, R. Blume, T. Rocha, D. Teschner, A. Knop-Gericke, R. Schlögl, N. Memmel, D. Zemlyanov, G. Rupprechter, and B. Klötzer, Angew. Chem., Int. Ed. **49**, 3224 (2010).
[19]C. Rameshan, C. Weilach, W. Stadlmayr, S. Penner, H. Lorenz, M. Havecker, R. Blume, T. Rocha, D. Teschner, A. Knop-Gericke, R. Schlögl, D. Zemlyanov, N. Memmel, G. Rupprechter, and B. Klötzer, J. Catal. **276**, 101 (2010).
[20]K. Kovnir, M. Armbrüster, D. Teschner, T. V. Venkov, L. Szentmiklósi, F. C. Jentoft, A. Knop-Gericke, Y. Grin, and R. Schlögl, Surf. Sci. **603**, 1784 (2009).
[21]W. Stadlmayr, V. Huber, S. Penner, B. Klötzer, and N. Memmel, J. Phys. Chem. C **117**, 19558 (2013).
[22]J. Osswald, R. Giedigkeit, R. E. Jentoft, M. Armbrüster, F. Girgsdies, K. Kovnir, T. Ressler, Y. Grin, and R. Schögl, J. Catal. **258**, 210 (2008).
[23]M. Friedrich, D. Teschner, A. Knop-Gericke, and M. Armbrüster, J. Catal. **285**, 41 (2012).
[24]P. Gille, T. Ziemer, M. Schmidt, K. Kovnir, U. Burkhardt, and M. Armbrüster, Intermetallics **18**, 1663 (2010).
[25]D. Rosenthal, R. Widmer, R. Wagner, P. Gille, M. Armbrüster, Y. Grin, R. Schlögl, and O. Gröning, Langmuir **28**, 6848 (2012).
[26]J. Prinz, R. Gaspari, C. A. Pignedoli, J. Vogt, P. Gille, M. Armbrüster, H. Brune, O. Gröning, D. Passerone, and R. Widmer, Angew. Chem. **124**, 9473 (2012).
[27]J. Prinz, R. Gaspari, Q. S. Stöckl, P. Gille, M. Armbrüster, H. Brune, O. Gröning, C. A. Pignedoli, D. Passerone, and R. Widmer, J. Phys. Chem. C **118**, 12260 (2014).
[28]C. Rameshan, H. Lorenz, L. Mayr, S. Penner, D. Zemlyanov, R. Arrigo, M. Hävecker, R. Blume, A. Knop-Gericke, R. Schlögl, and B. Klötzer, J. Catal. **295**, 186 (2012).
[29]G. M. McGuirk, J. Ledieu, É. Gaudry, M.-C. de Weerd, and V. Fournée, J. Chem. Phys. **141**, 084702 (2014).
[30]É. Gaudry, G. M. McGuirk, J. Ledieu, and V. Fournée, J. Chem. Phys. **141**, 084703 (2014).
[31]R. Franchy and G. Schmitz, EPL **51**, 534 (2000).
[32]M. Hahne and P. Gille, J. Cryst. Growth **401**, 622 (2014).
[33]H. Okamoto, J. Phase Equilib. **24**, 481 (2003).
[34]E. Bauer, Surf. Rev. Lett. **5**, 1275 (1998).
[35]E. Bauer, J. Electron Spectrosc. Relat. Phenom. **114-116**, 975 (2001).
[36]S. S. Dhesi, S. A. Cavill, A. Potenza, H. Marchetto, R. A. Mott, P. Steadman, A. Peach, E. L. Shepherd, X. Ren, U. H. Wagner, and R. Reininger, AIP Conf. Proc. **1234**, 311 (2010).
[37]A. Mayer, H. Salopaasi, K. Pussi, and R. D. Diehl, Comput. Phys. Commun. **183**, 1443 (2012).
[38]M. A. VanHove, W. Moritz, H. Over, P. J. Rous, A. Wander, A. Barbieri, N. Materer, U. Starke, and G. A. Somorjai, Surf. Sci. Rep. **19**, 191 (1993).
[39]J. B. Pendry, J. Phys. C: Solid State Phys. **13**, 937 (1980).
[40]A. Barbieri and M. A. Van Hove, private communication (2014).
[41]Y. Gauthier, R. Baudoing, and A. E. Miller, *Segregation and Related Phenomena* (University of Louisville, 2008).
[42]C. J. Powell and A. Jablonski, Nucl. Instrum. Methods Phys. Res., Sect. A **601**, 54 (2009).
[43]S. Tanuma, C. J. Powell, and D. R. Penn, Surf. Interface Anal. **43**, 689 (2011).
[44]See supplementary material at http://dx.doi.org/10.1063/1.4928650 for showing a LEED movie of the InPd(110) surface after annealing at 970 K where the primary beam energy varies from 20 to 250 ev.
[45]J. C. Slater, J. Chem. Phys. **41**, 3199 (1964).
[46]J. R. Noonan and H. L. Davis, Phys. Rev. Lett. **59**, 1714 (1987).
[47]M. Wencka, M. Hahne, A. Kocjan, S. Vrtnik, P. Kozelj, D. Korze, Z. Jaglicic, M. Soric, P. Popcevic, J. Ivkov, A. Smontara, P. Gille, S. Jurga, P. Tomes, S. Paschen, A. Ormeci, M. Armbrüster, Y. Grin, and J. Dolinsek, Intermetallics **55**, 56 (2014).
[48]M. Hahne and P. Gille, "Off-stoichiometric InPd single crystals by In-rich solution growth and post-growth annealing" (unpublished).
[49]C. Jiang, L.-Q. Chen, and Z.-K. Liu, Intermetallics **14**, 248 (2006).
[50]D. Ivarsson, M. Neumann, A. Levin, T. Keilhauer, P. Wochner, and M. Armbrüster, Z. Anorg. Allg. Chem. **640**, 3065 (2014).
[51]H. Lorenz, S. Turner, O. I. Lebedev, G. V. Tendeloo, B. Klöltzer, C. Rameshan, K. Pfaller, and S. Penner, Appl. Catal., A **374**, 180 (2010).
[52]J. R. Kitchin, K. Reuter, and M. Scheffler, Phys. Rev. B **77**, 075437 (2008).
[53]M. Krajci and J. Hafner, J. Catal. **312**, 232 (2014).
[54]F. Bechstedt, *Principles of Surface Physics* (Springer, 2003).
[55]S. Kurth, J. P. Perdew, and P. Blaha, Int. J. Quantum Chem. **75**, 889 (1999).
[56]Z.-X. Chen, K. M. Neyman, A. B. Gordienko, and N. Rösch, Phys. Rev. B **68**, 075417 (2003).
[57]J. Hafner and M. Kraj, Acc. Chem. Res. **47**, 3378–3384 (2014).